The potential of a large dust grain in a collisionless plasma

Dogan Akpinar and George E. B. Doran

August 12, 2020

Abstract

Abstract goes here

1 Introduction

2 Background

In the case of a large dust grain with a negative equilibrium charge, we can establish regions within an infinite plasma with well-defined transitions. We firstly have the dust grain itself, followed by an electron deficient region, called the sheath, usually a few electron Debye lengths in size. The electron Debye length is a characteristic length over which quasi-neutrality breaks down [1] [2], defined as

$$\lambda_D = \sqrt{\frac{\varepsilon_0 k_B T_e}{n_0 e^2}}, \tag{1}$$

where k_B is the Boltzmann constant, T_e is the electron temperature, e is the electron charge, n_0 is the electron number density at infinity and ε_0 is the permittivity of free space. Following the sheath, there exists the infinite pre-sheath where quasi-neutrality holds; quasi-neutrality can be expressed as an approximate equality between the ion and electron densities, $Zn_i \approx n_e$ [2].

Positive ions are continuously collected by the negative dust, so there must be a net influx of ions into the sheath to maintain the equilibrium. This establishes the Bohm criterion [3], where the speed of the ions required to enter the sheath must be greater than or equal to the Bohm speed. For the cold ion case, the Bohm speed is defined as

$$c_s^{cold} = \sqrt{\frac{k_B T_e}{m_i}}, \tag{2}$$

where m_i is the ion mass and c_s^{cold} is known as the cold ion Bohm speed. However, if we consider ions with a finite temperature, the required Bohm speed becomes

$$c_s^{hot} = \sqrt{\frac{k_B(T_e + \gamma T_i)}{m_i}}, \tag{3}$$

where T_i is the ion temperature, γ is the adiabatic index and c_s^{hot} is known as the hot ion Bohm speed [4] [5] .

For a large dust grain, we may consider the planar sheath (thin sheath) limit [5]. Hence, the potential drop across the sheath for $T_i \neq 0$ is given as

$$\phi_s = \frac{k_B T_e}{2e} \ln\left[\frac{2\pi Z^2}{\mu^2}(1 + \gamma\Theta)\right], \tag{4}$$

where Z is the relative ion charge, $\mu = \sqrt{\frac{m_i}{m_e}}$ and $\Theta = \frac{T_i}{T_e}$ [4].

3 Radial motion theory (ABR)

The ABR model is a radial motion theory derived by Allen, Boyd and Reynolds. It describes the equilibrium surface potential acquired by a dust grain immersed in an infinite and stationary plasma [6].

Consider a spherical dust grain, of arbitrary radius a, immersed in this infinite plasma. Far from the surface we assume that the electron and ion densities are equal, denoted n_e and n_i respectively; this is known as quasi-neutrality. As electrons are faster than ions, it can be shown that such a dust grain will become negatively charged [7], thus ions will experience an attractive force due to the potential on the dust surface, ϕ_a. We assume that ions at infinity have no kinetic energy, hence, they move radially towards the dust grain. Therefore, it is appropriate to say that an ion at a distance r from the dust center has radial speed v_i. Using energy conservation, one can show the following,

$$\frac{1}{2} m_i v_i^2 = -Ze\phi(r), \tag{5}$$

where $\phi(r)$ is the potential at r, which vanishes as $r \to \infty$ [6].

Equation (5) then leads to an expression for the ion current, which is entirely dependant on the radial distance from the dust grain, given by

$$I_i = \frac{4\sqrt{2}\ n_i \pi r^2 Z^{\frac{3}{2}} e^{\frac{3}{2}} \phi_a^{\frac{1}{2}}}{m_i^{\frac{1}{2}}}. \tag{6}$$

As the potential is negative, few electrons reach the dust grain, hence, the electron density obeys a Boltzmann distribution:

$$n_e(r) = n_0 \exp\left(\frac{e\phi(r)}{k_B T_e}\right), \tag{7}$$

we further assume that only inbound electrons contribute to the electron current at the surface of the dust grain, given as

$$I_i = I_e = 4\pi a^2 n_0 e \sqrt{\frac{k_B T_e}{2\pi m_e}} \exp\left(\frac{e\phi_a}{k_B T_e}\right). \tag{8}$$

where m_e is the electron mass [6].

It is useful to apply the following normalisations, noting that Φ is the opposite sign for simplicity:

$$\Phi = -\frac{e\phi}{k_B T_e},\ \rho = \frac{r}{\lambda_D},\ \alpha = \frac{a}{\lambda_D},\ J = \frac{I_i}{4\pi\lambda_D^2 n_0 e\sqrt{\frac{2k_B T_e}{m_i}}}, \tag{9}$$

where λ_D is the electron Debye length,

Poisson's law allows for the formation of a differential equation which relates the spatial variation of the potential to the difference in electron and ion densities,

$$\frac{d}{d\rho}\left(\rho^2 \frac{d\Phi}{d\rho}\right) = JZ^{-\frac{1}{2}}\Phi^{-\frac{1}{2}} - \rho^2 \exp(-\Phi). \tag{10}$$

This equation may be solved using the boundary conditions;

$$\rho \approx J^{\frac{1}{2}} Z^{-\frac{1}{4}} \Phi^{-\frac{1}{4}} \exp\left(\frac{\Phi}{2}\right), \tag{11}$$

$$\left.\frac{d\Phi}{d\rho}\right|_{\rho_b} = \frac{2\rho_b Z^{\frac{1}{2}} J^{-1} \Phi_b^{\frac{3}{2}}}{\Phi_b - \frac{1}{2}} exp(-\Phi_b), \tag{12}$$

$$\frac{J}{\Gamma} = \frac{4Z^{\frac{1}{2}}\Phi_b^{\frac{3}{2}}(2\Phi_b - 3)(2\Phi_b + 1)}{(2\Phi_b - 1)^3}, \tag{13}$$

$$\frac{J}{\alpha^2} = \frac{\mu}{\sqrt{4\pi}} \exp(-\Phi_a), \tag{14}$$

which are formed by assuming that there exists a certain distance ρ_b, past which, quasi-neutrality applies. The potential at ρ_b is given by Φ_b, and Γ is a number much greater than unity [6]. In order to find a value for the surface potential we must solve (10), this may be achieved using a 4th order Runge-Kutta. We choose $\Gamma = 10000$ and find the roots of (13) allowing us to determine the necessary boundary conditions using (11) and (12). Hence, solving the differential equation numerically, yields the following graph of normalised dust potential as a function of normalised dust radius.

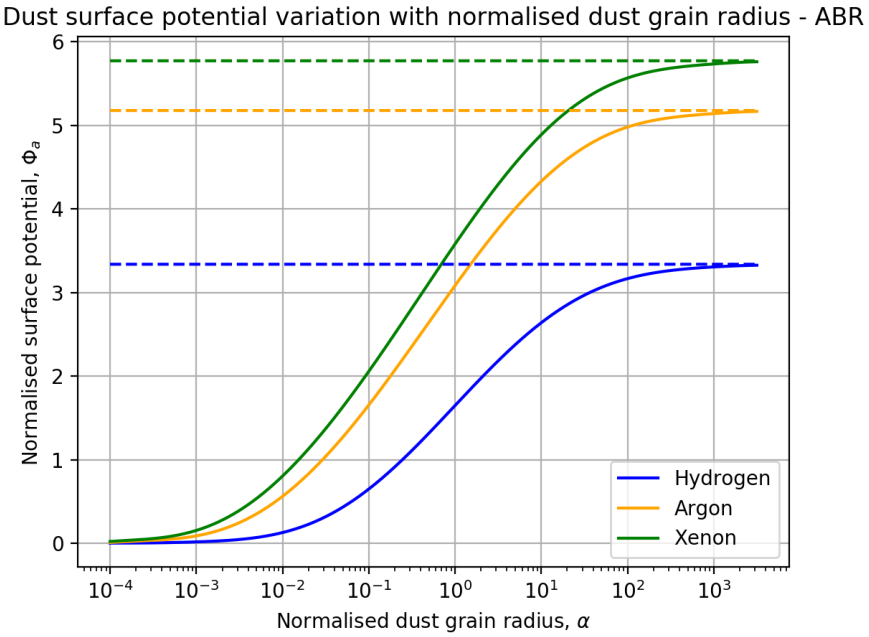

Figure 1: ABR predictions for Φ_a as a function of α for a dust grain in singly ionised Hydrogen, Argon and Xenon plasmas ($Z = 1$) [6] [7].

Thomas discusses that in the limit of $\alpha \to \infty$ the ABR potential approaches the cold planar wall limit [7], given as the following

$$\lim_{\alpha \to \infty} \Phi_a = \frac{1}{2} \ln (2\pi) - \frac{1}{2} - \ln (\mu), \tag{15}$$

where $Z = 1$ and the $-\frac{1}{2}$ is due to the potential drop across the cold ion presheath, as discussed by Stangeby [4] [8]. Furthermore, one can clearly see that in the limit of $\alpha \to 0$ the ABR prediction tends to zero also [6].

4 Modified orbital motion limited (MOML)

Orbital motion limited (OML) models the potential, ϕ_a, on a small spherical dust grain immersed in an infinite and collisionless plasma, it does so by considering energy and angular momentum conservations of the ions along side a critical grazing incidence. OML considers an equilibrium of ion and electron currents at the dust surface, $I_i = I_e$, while simultaneously invoking quasi-neutrality [9]. Hence, the standard result acquired from OML is the following

$$\frac{\sqrt{\Theta}}{\mu} \left(1 - \frac{Z}{\Theta} \Phi_a \right) \approx \exp (\Phi_a), \tag{16}$$

where $\Phi_a = \frac{e\phi_a}{k_B T_e}$.

Using available OM data, Willis discusses that any error in OML is negligible for small dust grains, he further proposes an upper radius limit for OML which is Θ dependant [5]. Furthermore, it should be noted that OML guarantees the existence of absorption radii, $r_A > a$, such that any ion within r_A approaching the dust grain will be collected [7].

In order to model a large dust grain, we must slightly change our approach to the problem. We now apply OML to the boundary between the sheath and pre-sheath, this establishes the assumption that as $\alpha \to \infty$ any ion that enters the sheath will be collected by the dust grain. For such dust grains, the majority of absorption radii occur within the sheath, hence, applying OML in this was eliminates most of the inaccuracies introduced by absorption radii and ensures the validity of MOML. However, it will be shown later that the validity of MOML in fact breaks down for small Θ [7].

Replacing Φ_a on the left hand side in (16) with Φ_s, the normalised potential at the sheath edge, physically amounts to saying that as $\alpha \to \infty$, all ions that enter the sheath are absorbed. Considering an equilibrium of electron and ion currents at the sheath edge while simultaneously invoking quasi-neutrality and the expression for the hot ion Bohm speed, (3), one acquires the following relationship between Φ_s and Φ_a

$$\Phi_s \approx \Phi_a - \frac{1}{2}\ln\left[\frac{2\pi Z^2}{\mu^2}(1+\gamma\Theta)\right], \tag{17}$$

where the second term is the normalised sheath potential drop, (4). Substituting (17) into the modified (16) and manipulating in terms of the the principle branch of the Lambert W function, W_0, yields

$$\Phi_a = \frac{\Theta}{Z} - W_0\left(\sqrt{2\pi\Theta(1+\gamma\Theta)}\exp\left(\frac{\Theta}{Z}\right)\right) + \frac{1}{2}\ln\left[\frac{2\pi Z^2}{\mu^2}(1+\gamma\Theta)\right]. \tag{18}$$

Willis compares the MOML solution with simulated data ran by PIC and concludes that $\gamma = \frac{5}{3}$ seems to produce the most appropriate predictions [5]. Hence, $\gamma = \frac{5}{3}$ is chosen as the default value for our investigation. It is worth noting that from (Fig. 2) we see that for extreme, and even intermediate, Θ values, the choice of γ has very little affect on the predicted potential.

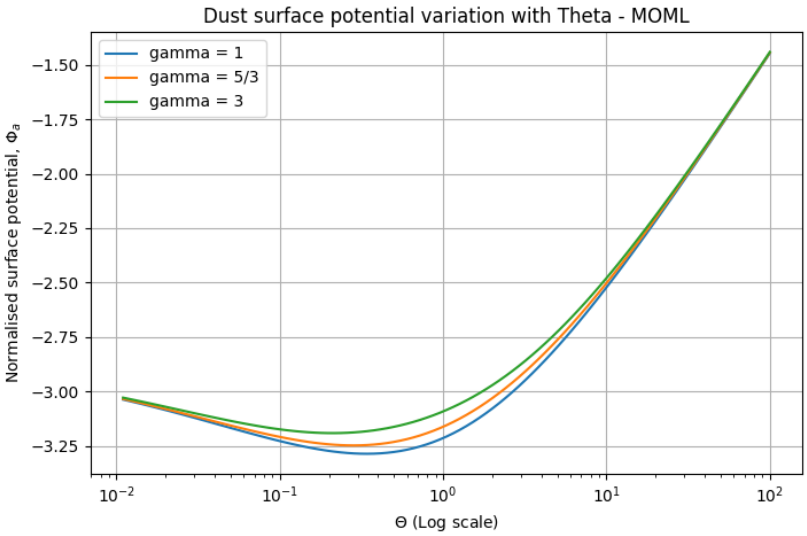

Figure 2: The MOML prediction for Φ_a as a function of Θ, for a hydrogenic ($\mu \approx 43$) and singly ionised ($Z = 1$) plasma with different values of γ [7].

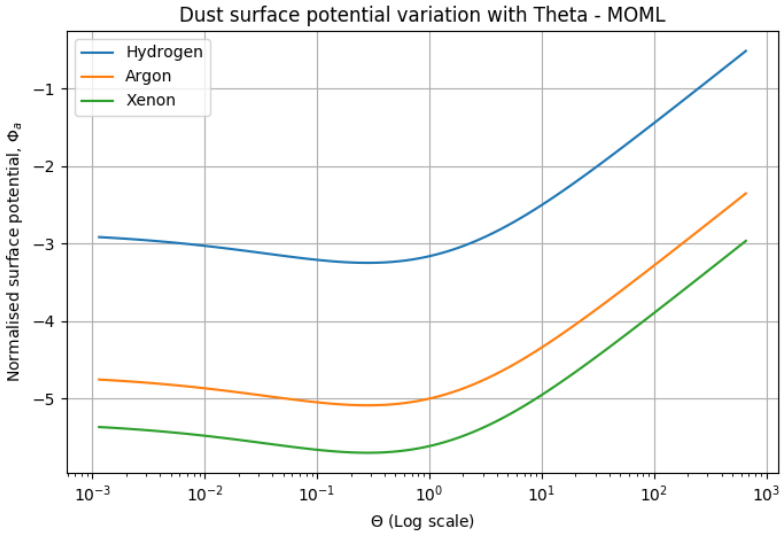

Figure 3: Normalised surface potential as a function of Θ for singly ionised ($Z = 1$) Hydrogen, Argon and Xenon plasmas according on the MOML prediction, plotted on a log-linear scale.

5 SCEPTIC numerical fit

SCEPTIC is used to investigate the charging of dust grains in a variety of plasma conditions. Willis discusses that SCEPTIC data has been compared to OM theory, and has shown that the agreement between the two is excellent over a large range of dust sizes for $\Theta = 0.01, 0.1, 1$ [10].

Upon further inspection of SCEPTIC data, Willis states that in the OML (small dust) and planar sheath (large dust) limits, the (normalised) potential, Φ_a, is independent of the (normalised) dust radius, α [10]. He further states that the data in these cases can be well fitted by the following expression

$$\Phi_a = \lambda \ln A + \eta \ln \Theta + C, \tag{19}$$

where A is the mass number of the ion species and λ, η, C are constants. In this section we will only consider the SCEPTIC fit for large dust grains; the following table summarises the values of λ, η and C for differing Θ ranges.

Table 1: SCEPTIC fit parameters for the planar sheath limit

	λ	η	C
$\Theta \leq 2$	0.456	0	3.179
$\Theta > 2$	0.557	$-0.386 - 0.024 \ln A$	3.399

6 Comparison between models for low ion temperature

It is well established that MOML agrees with SCEPTIC data, and by extension OM theory, for finite Θ values. However, for values of $\Theta < 1$, MOML seems to breakdown and deviate from ABR and OM theory.

Before explicitly comparing the models discussed until now, it should be noted that there is no available OM data for $\Theta < 0.01$, hence, we do not exactly know the predicted OM values for a plasma with such conditions. This is entirely due to the complexity of the theory itself and the limitation of numerical techniques available to solve its equations with certainty.

We may compare ABR and MOML in their respective limits to see if they are in agreement with one another, which is what we would expected. If we consider ABR in the limit of $\alpha \to \infty$ we recover the cold planar wall limit as shown in section 3, this value, for a singly charged hydrogenic plasma, is approximately -3.34. If we now consider the MOML solution, (18), in the cold ion limit with $Z = 1$, we attain the following

$$\lim_{\Theta \to 0} \Phi_a = \frac{1}{2} \ln (2\pi) - \ln (\mu). \tag{20}$$

This shows a discrepancy between ABR and MOML, when MOML is used to describe a cold ion plasma. As the ABR limit recovers well known and accepted values for the potential drop across a cold plasma in the planar sheath limit [4] [8], this result essentially invalidates MOML in the cold ion limit.

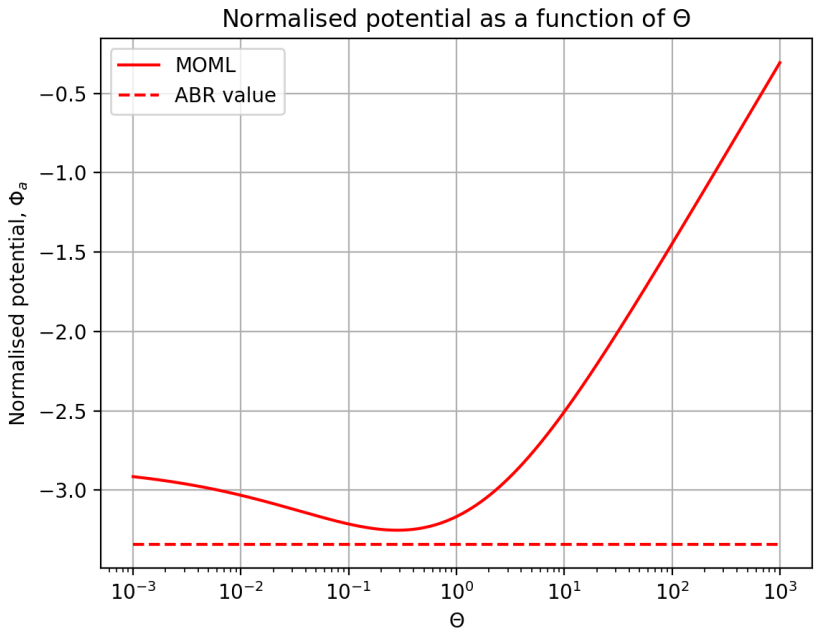

Figure 4: Normalised potential as a function of Θ for a singly charged hydrogenic plasma. We in fact see that in the limit of $\Theta \to 0$ MOML does not agree with ABR.

Upon further investigation, one sees that in the cold ion limit, MOML predicts a zero potential drop across the pre-sheath, where we expect it to be $-\frac{1}{2}$ [4]. It is believed that this discrepancy arises due to the existence of absorption radii well into the pre-sheath for low Θ, which is a result of applying OML at the sheath edge. Hence, we conclude that MOML is incorrect for $\Theta \to 0$.

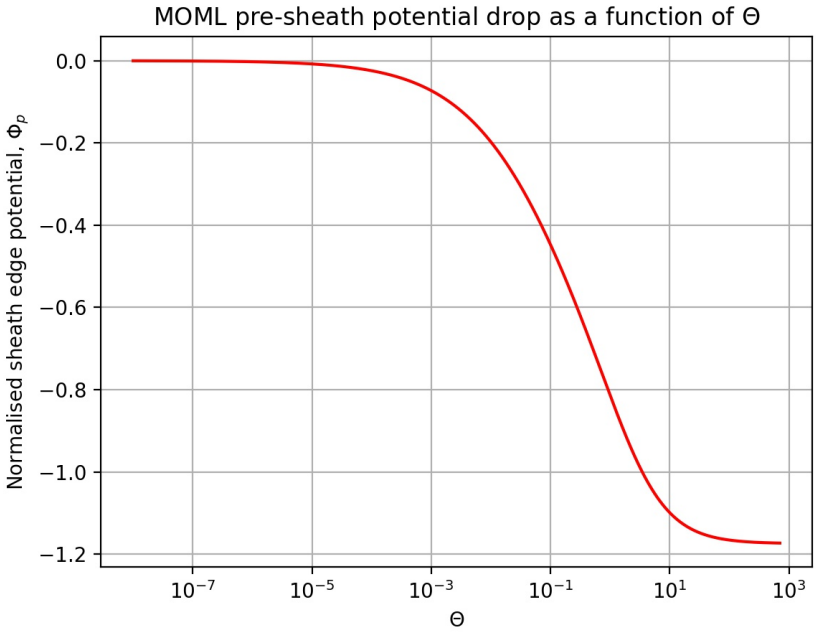

Figure 5: Pre-sheath potential drop as a function of Θ for a singly charged hydrogenic plasma as predicted by MOML.

7 Flowing sheath approximation

We are now posed with the task of finding an analytic solution for the potential on a large dust grain which is valid for low Θ. The approach we will take assumes the same electron behaviour as existing models [5], however, we will change the way in which the ions are modelled.

Our approach essentially considers each region of the plasma separately; we already know an analytic solution for the potential drop across a planar sheath for finite ion temperatures. However, in order to find the total potential drop across the plasma, we we must determine a temperature dependant potential drop across the pre-sheath.

We consider ions at infinity with an average energy of $E_0 = \kappa k_B T_i$, where κ is a constant to be determine. We now assume that the ions are modelled by a flowing Maxwellian at the sheath edge, with drift speed u,

$$f_i(\underline{\mathbf{v}}) = \left(\frac{m_i}{2\pi k_B T_i}\right)^{\frac{3}{2}} \exp\left(\frac{-m_i}{2k_B T_i}|\underline{\mathbf{v}} - \underline{\mathbf{u}}|^2\right). \tag{21}$$

In order to find the potential drop across the pre-sheath, we must determine

the average ion energy at the sheath edge, so we consider the following integral

$$\langle E_s \rangle = \frac{1}{2} m_i \int v^2 f_i(\underline{\mathbf{v}})\, d^3\underline{\mathbf{v}}. \tag{22}$$

For convenience, we will drop the subscripts for the time being, change to spherical polar coordinates and let $\xi = \frac{m_i}{2k_B T_i}$, yielding,

$$\langle E_s \rangle = \frac{1}{2} m \left(\frac{\xi}{\pi}\right)^{\frac{3}{2}} \int v^4 \sin\theta \exp\left(-\xi v^s - \xi u^2 + 2uv\xi\cos\theta\right) dv d\theta d\varphi, \tag{23}$$

where θ and φ are the polar and azimuthal angle respectively. We continue in the following way

$$\langle E_s \rangle = \pi m \left(\frac{\xi}{\pi}\right)^{\frac{3}{2}} \exp\left(-\xi u^2\right) \int_{v=0}^{\infty} v^4 \exp\left(-\xi v^2\right) \int_{\theta=0}^{\pi} \sin\theta \exp\left(2uv\xi\cos\theta\right) d\theta dv, \tag{24}$$

$$\langle E_s \rangle = \frac{\pi m}{u\xi} \left(\frac{\xi}{\pi}\right)^{\frac{3}{2}} \exp\left(-\xi u^2\right) \int_{v=0}^{\infty} v^3 \exp\left(-\xi v^2\right) \sinh\left(2uv\xi\right)\, dv, \tag{25}$$

but

$$\int_{v=0}^{\infty} v^3 \exp\left(-\xi v^2\right) \sinh\left(2uv\xi\right)\, dv = \frac{u\sqrt{\pi}}{4\xi^{\frac{3}{2}}} \left(2\xi u^2 + 3\right) \exp\left(\xi u^2\right). \tag{26}$$

Substituting (26) into (23) yields the average energy in terms of ξ and u

$$\langle E_s \rangle = \frac{1}{2} k_B T_i \left(2\xi u^2 + 3\right). \tag{27}$$

Ions at the sheath edge must satisfy the hot ion Bohm criterion, $u \geq c_s^{hot}$. Choosing $u = c_s^{hot}$ amounts to saying that the average speed at the sheath edge is the hot ion Bohm speed. Hence, the average ion energy at the sheath becomes,

$$\langle E_s \rangle = \frac{1}{2} k_B T_e \left(1 + \Theta\left(\gamma + 3\right)\right), \tag{28}$$

Using energy conservation across the pre-sheath,

$$E_0 - \langle E_s \rangle = Ze\phi_p, \tag{29}$$

then subbing in expressions for E_0, $\langle E_s \rangle$ and rearranging for ϕ

$$Ze\phi_p = \kappa k_B T_i - \frac{1}{2} k_B T_e \left(1 + \Theta\left(\gamma + 3\right)\right), \tag{30}$$

normalising yields,

$$\Phi_p = -\frac{1}{2Z}\left(1 + \Theta\left(\gamma + 3 - 2\kappa\right)\right), \tag{31}$$

which is the temperature dependant pre-sheath potential drop. When $\Theta = 0$ we recover the potential drop across a cold pre-sheath [4].

Therefore, we may determine the total potential drop across the plasma, by summing the known Φ_s with the newly determined Φ_p, given by the following equation

$$\Phi_a = \frac{1}{2}\ln\left[\frac{2\pi Z^2}{\mu^2}(1 + \gamma\Theta)\right] - \frac{1}{2Z}\left(1 + \Theta\left(\gamma + 3 - 2\kappa\right)\right). \tag{32}$$

where $\gamma = \frac{5}{3}$ and κ is still to be determined.

7.1 Choosing the value of κ

The value of κ is sensitive to the choice of distribution function at infinity. In this section we suggest two possible functions and discuss their effects on the expected results in the region of interest, $0 \leq \Theta \leq 1$.

7.1.1 $\kappa = \frac{3}{2}$

Given a flowing Maxwellian at the sheath edge, it would be logical to assume a static Maxwellian at infinity. In doing so, we find the average ion energy to be $E = \frac{3}{2}k_B T_i$.

Analysing figure (6) shows that the model agrees with ABR in the cold ion limit, which is the behaviour we expect. However, as Θ approaches 1, the predicted potential actually decreases and the percentage error of the model compared to the SCEPTIC fit becomes worse than MOML. Suggesting that, despite $\kappa = \frac{3}{2}$ being the best choice for consistency with our assumption at the sheath edge, the model fails to predict the expected behaviour in the region of interest with said κ.

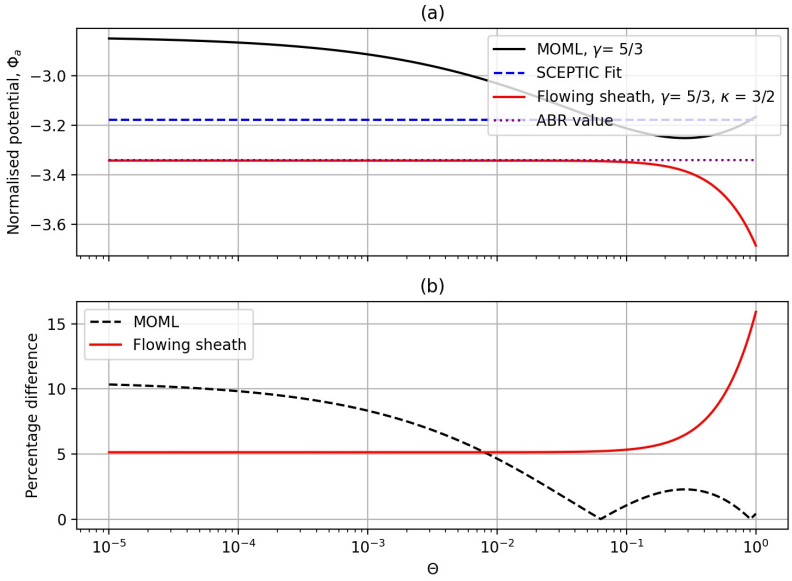

Figure 6: (a) Variation of normalised potential with Θ for a singly charged hydrogenic plasma using MOML, SCEPTIC, ABR and the flowing sheath approximation with $\kappa = \frac{3}{2}$. (b) Percentage difference between MOML, flowing sheath approximation and the SCEPTIC fit with $\kappa = \frac{3}{2}$.

7.1.2 $\kappa = 2$

We now consider a different distribution function at infinity, which would be a result of changing our choice for the ion source function. Stangeby presents two potential candidates for the ion source function at infinity, the first being the standard Maxwellian, as discussed in the previous subsection, and the second being a non Maxwellian distribution presented by Emmert et al. [11] given as

$$S(x, v_x) = S_p(x) \left(\frac{m_i |v_x|}{2k_B T_i} \right) \exp \left(\frac{-m_i |v_x|^2}{2k_B T_i} \right). \tag{33}$$

Stangeby discusses that upon further analysis, one may find that the average ion energy according to this distribution in 3D is in fact $E = 2k_B T_i$.

Surprisingly, when fitting the flowing sheath approximation to available SCEPTIC data, one finds that the optimal choice for κ is 2.1, hence, for the remainder of the analysis we will choose $\kappa = 2$. However, it should be noted that the reason as to why and how the ion distribution function changes across the pre-sheath, as suggested by this model, is still unknown.

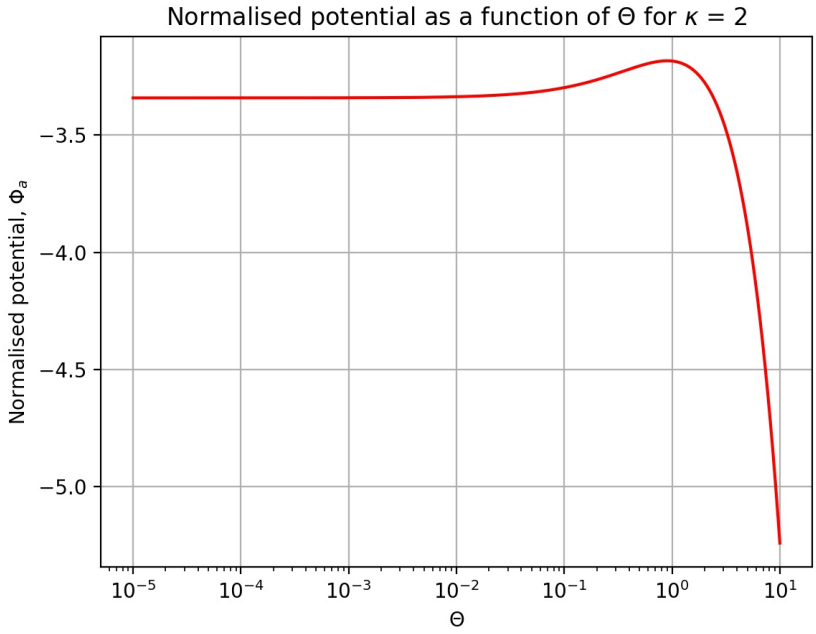

Figure 7: Normalised potential as a function of Θ for a singly charged hydrogenic plasma using the newly determined model with $\kappa = 2$.

7.1.3 The flowing sheath approximation as a lower bound

Figure (7) (section 7.1.2) shows the predicted dust potential as a function of Θ for the model with $\kappa = 2$. We see that for values of $\Theta \leq 1$ the potential seems reasonable, however, for higher values of Θ the model seems to completely diverge from MOML. Initially, when seeing this behaviour one may become sceptical of the model, however, it should be noted that we have assumed the average ion speed at the sheath edge to be c_s^{hot}. It is very likely that the average ion speed at the sheath edge is not c_s^{hot}, but in fact greater than c_s^{hot}. Hence, our assumption does not account for the possibility of the average ion speed being greater than c_s^{hot}.

In order to account for such a possibility, noting that our solution for Φ_a is monotonically decreasing, we must consider that $u \geq c_s^{hot}$, yielding a lower bound for the average ion energy at the sheath edge

$$\langle E_s \rangle \geq \frac{1}{2} k_B T_i \left(2\xi u^2 + 3\right). \tag{34}$$

Following the same steps as (28) through (31) we determine that

$$\Phi_a \geq \frac{1}{2}\ln\left[\frac{2\pi Z^2}{\mu^2}(1+\gamma\Theta)\right] - \frac{1}{2Z}\left(1+\Theta\left(\gamma+3-2\kappa\right)\right), \tag{35}$$

suggesting that the potential predicted by this model acts as a lower bound for the dust grain potential.

7.2 Validity range for the flowing sheath approximation

In order to determine the reliability of the model, we must compare it to existing models that are accepted within the plasma community. As stated before, we know that the new model deviates from MOML for values of $\Theta > 1$; however, the MOML potential is in fact greater than the potential predicted by the model in this region, and so is above the lower bound that the model imposes. Therefore, for values of $\Theta > 1$, MOML is still the most appropriate model available.

The most interesting behaviour of the model is seen for $\Theta \leq 1$. In the limit of $\Theta \to 0$ the model exactly recovers the ABR value and so rectifies the discrepancy between MOML and ABR. Furthermore, the value predicted for $\Theta = 1$ is the same as that predicted by OM theory for $\alpha = 100$ and $\Theta = 1$, suggesting that the model exactly reproduces known values for the extreme values of $0 \leq \Theta \leq 1$. Within the region of interest, we see that the model predicts an increasing potential from the ABR value, as is expected, in direct contrast to a decreasing potential from a wrong cold ion value as suggested by MOML.

Upon further analysis, as shown in figure (8), we have determined that in this range the flowing sheath approximation has, on average, a smaller percentage difference from the SCEPTIC fit. Therefore, If we assume the SCEPTIC fit to be correct for $\Theta \to 0$, ignoring its discrepancy from ABR, we find that the flowing sheath approximation is the better model in this range. Thus providing sufficient evidence to replace MOML with the flowing sheath approximation for these values of Θ.

Therefore, the new proposed potential on a large dust grain in a finite ion temperature plasma is given as follows

$$\Phi_a = \begin{cases} \frac{1}{2}\ln\left[\frac{2\pi Z^2}{\mu^2}(1+\gamma\Theta)\right] - \frac{1}{2Z}\left(1+\Theta\left(\gamma+3-2\kappa\right)\right) & \text{for } 0 \leq \Theta \leq 1 \\ \frac{\Theta}{Z} - W_0\left(\sqrt{2\pi\Theta(1+\gamma\Theta)}\exp\left(\frac{\Theta}{Z}\right)\right) + \frac{1}{2}\ln\left[\frac{2\pi Z^2}{\mu^2}(1+\gamma\Theta)\right] & \text{for } \Theta > 1 \end{cases} \tag{36}$$

where $\gamma = \frac{5}{3}$ and $\kappa = 2$ give the best results.

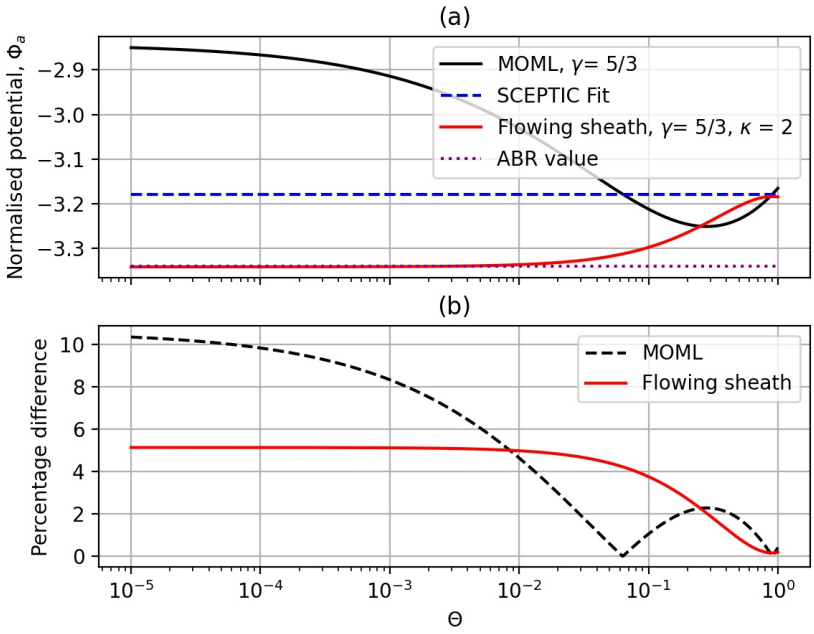

Figure 8: (a) Variation of normalised potential with Θ for a singly charged hydrogenic plasma using MOML, SCEPTIC, ABR and the flowing sheath approximation. (b) Percentage difference between MOML, flowing sheath approximation and the SCEPTIC fit.

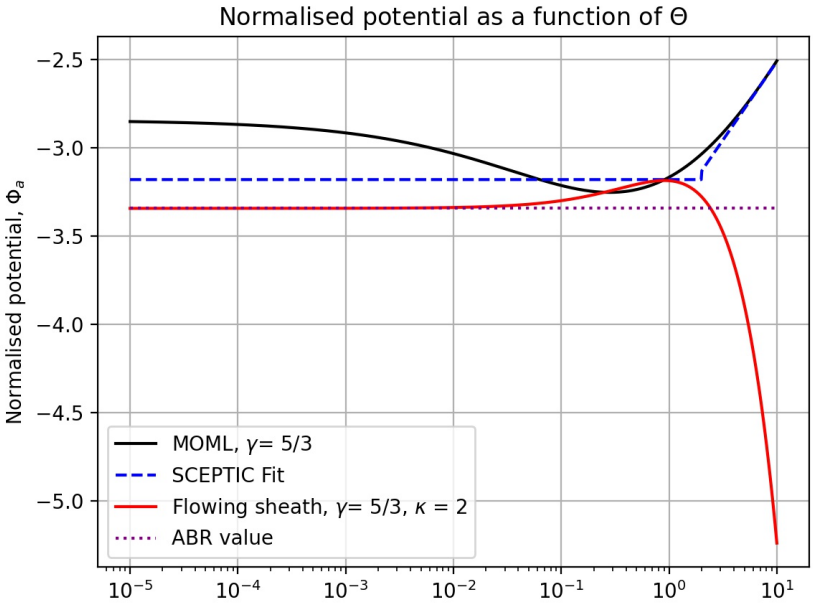

Figure 9: Normalised potential as a function of Θ for a singly charged hydrogenic plasma using MOML, SCEPTIC, ABR and the flowing sheath approximation for $0 \leq \Theta \leq 10$.

8 Conclusion

9 References and Acknowledgements

[1] N. Hershkowitz, "Sheaths: More complicated than you think," *Physics of Plasmas*, vol. 12, no. 5, p. 055502, 2005. [Online]. Available: https://doi.org/10.1063/1.1887189

[2] K. Wiesemann, "A Short Introduction to Plasma Physics," in *CAS - CERN Accelerator School: Ion Sources*, 2013, pp. 85–122.

[3] L. Kos, D. D. Tskhakaya, and N. Jelić, "Unified bohm criterion," *Physics of Plasmas*, vol. 22, no. 9, p. 093503, 2015. [Online]. Available: https://doi.org/10.1063/1.4930207

[4] P. C. Stangeby, *The Plasma Sheath*. Boston, MA: Springer US, 1986, pp. 41–97. [Online]. Available: https://doi.org/10.1007/978-1-4757-0067-1_3

[5] C. T. N. Willis, "Dust in stationary and flowing plasmas," Physics PhD Thesis, Imperial College London, March 2012.

[6] K. R. V. and A. J. E., "The floating potential of spherical probes and dust grains. part 1. radial motion theory," *Journal of Plasma Physics*, vol. 67.4, pp. 243–50, 2002.

[7] D. M. Thomas, "Theory and simulation of the charging of dust in plasmas," Physics PhD Thesis, Imperial College London, March 2016.

[8] P. Stangeby, *The Plasma Boundary of Magnetic Fusion Devices*, ser. Series in Plasma Physics and Fluid Dynamics. Taylor & Francis, 2000. [Online]. Available: https://books.google.co.uk/books?id=qOliQgAACAAJ

[9] M.-S. H. and L. I., "The theory of collectors in gaseous discharges," *Physical Review*, vol. 28(4), pp. 727–763, 1926.

[10] C. T. N. Willis, M. Coppins, M. Bacharis, and J. E. Allen, "The effect of dust grain size on the floating potential of dust in a collisionless plasma," *Plasma Sources Science and Technology*, vol. 19, no. 6, p. 065022, nov 2010. [Online]. Available: https://doi.org/10.1088%2F0963-0252%2F19%2F6%2F065022

[11] G. Emmert, R. Wieland, A. Mense, and J. Davidson, "Electric sheath and presheath in a collisionless, finite ion temperature plasma," *Physics of Fluids*, vol. 23, 04 1980.

10 Appendix

10.1 Symbol dictionary

e	Electron charge
ε_0	Permittivity of free space
k_B	Boltzmann's constant
a	Dust radius
α	Normalised dust radius
$_a$	Subscript indicating a quantity at the dust grain surface
r	Distance from the centre of the dust grain
ρ	Normalised distance from the centre of the dust grain
λ_D	Debye length
m_j	Mass
n_j	Density
T_j	Temperature
I_j	Current
$_j$	Subscript indicating a plasma particle
$_i$	Subscript indicating an ion quantity
$_e$	Subscript indicating an electron quantity
$_0$	Subscript indicating an electron quantity at infinity
μ	Root mass ratio
Θ	Ratio of ion to electron temperature
γ	Heat capacity ratio
u	Flow velocity
υ	Normalised flow velocity
Γ	ABR correction factor
Z	Ion charge number
Q	Dust grain charge
ϕ	Electric potential
Φ	Normalised electric potential